MODELING STIMULUS-FREQUENCY OTOACOUSTIC EMISSIONS IN THE GECKO

CHRISTOPHER BERGEVIN

Department of Mathematics, University of Arizona,
Tucson, Arizona 85705 USA

CHRISTOPHER A. SHERA

Eaton-Peabody Laboratory,
Massachusetts Eye & Ear Infirmary,
Boston, Massachusetts 02114 USA

Although lizards lack the basilar-membrane traveling waves evident in mammals, their ears produce stimulus-frequency otoacoustic emissions (SFOAEs) with latencies comparable to those measured in many mammals (1–2 ms or greater). To probe the origin of these relatively long OAE delays, we developed a model of SFOAE generation in the gecko. The model inner ear comprises a collection of linear, coupled oscillators (hair bundles and associated tectorium) whose effective damping manifests a small degree of irregularity. The model reproduces the major qualitative features of gecko SFOAEs, including their substantial delays. The SFOAE delays predicted by the model increase with the assumed sharpness of tuning, reflecting the build-up time associated with mechanical resonance.

1. Introduction

Stimulus-frequency otoacoustic emissions (SFOAEs) exhibit significant phase-gradient delays in both mammalian [1] and non-mammalian ears [2]. Although mammalian SFOAE delays are often attributed to basilar-membrane (BM) traveling waves, the origin of the delay in non-mammals, especially those lacking BM waves, remains unclear. Here we explore the origin of OAE delay in the gecko, a species in which SFOAE phase-gradient delays are 1–2 ms or greater, comparable to those measured in many mammals. Lizard ears lack BM traveling waves [3], and their tuning and tonotopy are thought to arise micromechanically at the level of the hair-cell bundle [4,5]. Our goal is to determine whether a simple model of the gecko inner ear—a collection of coupled oscillators representing the hair bundles, associated structures, and adjacent fluid—can account for measured SFOAE delays.

2. The Model

We simplify the gecko inner ear morphology as shown in Fig. 1. Middle-ear delays are assumed negligible [6]. The model consist of two rigid-walled cavities (the scala vestibuli and tympani) filled with incompressible fluid and separated by the papilla. The papilla is assumed to vibrate as a rigid body in the transverse direction only, driven by the pressure difference $(P_v - P_t)$ between the two scalae. The scalae pressures P_v and P_t are assumed uniform at the frequencies of interest. The papilla and the hair cells on its surface are represented by linear oscillators (i.e., masses,
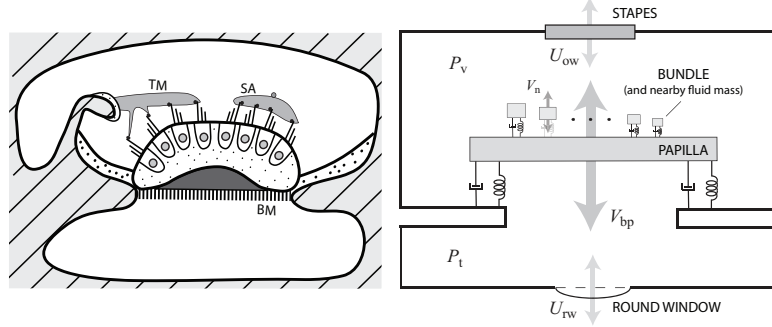
Fig. 1: *Left:* Simplified transverse-radial cross-sectional schematic of the gecko inner-ear anatomy showing hair cells embedded in the papilla. The papilla has an effective area $A_{\rm bp}$ and length L (~ 1 cm). The gecko is one of many lizard species with sallets, discretized sections of tectorium that are thought to behave as resonant filters. White regions are fluid-filled, gray region represent the overlying tectorium, gray striped areas represent bone, and stippled areas are supporting cellular structures. Abbreviations: BM–basilar membrane, TM–tectorial membrane, SA–sallet. *Right:* Longitudinal-transverse cross-section of the model, consisting of a collection of n linear oscillators coupled only by the motion of the basilar papilla.

springs, and dashpots). We assume harmonic time dependence and represent dynamical variables by Fourier coefficients at angular (driving) frequency ω.

By analogy with models of mammalian OAEs, SFOAEs are produced by introducing micromechanical irregularity [7]. Studies of lizard inner-ear anatomy [8,9] show irregular variations in features such as the width and thickness of the BM and basilar papilla, the number of hair cells in a given radial cross-section, and the coupling between the hair bundles and overlying tectorium. We quantify the emission as the pressure $\Delta P(\omega)$, defined by

$$\Delta P(\omega) \equiv \left[\tilde{Z}(\omega) - Z(\omega) \right] U_{\rm ow} \ , \tag{1}$$

where $U_{\rm ow}$ is the stapes volume velocity, $\tilde{Z}(\omega)$ and $Z(\omega)$ are the cochlear input impedances $[(P_{\rm v} - P_{\rm t})/U_{\rm ow}]$ computed with and without micromechanical irregularity, respectively.

We compute the input impedance by solving the equations of motion for the system. Newton's second law implies that

$$Z_{\rm bp}V_{\rm bp} = A_{\rm bp}(P_{\rm v} - P_{\rm t}) + \sum_n \frac{k_n}{i\omega} \left(V_n - V_{\rm bp} \right) \ . \tag{2}$$

In this equation, $V_{\rm bp}$ is the transverse velocity of the papilla, and $A_{\rm bp}$ and $Z_{\rm bp}$ are its effective cross-sectional area and mechanical impedance, respectively. V_n and k_n represent the velocity and effective stiffness of the nth hair bundle. The individual bundles are coupled only through the motion of the underlying papilla and satisfy the equation

$$i\omega m_n V_n = -r_n V_n - \frac{k_n}{i\omega}(V_n - V_{\rm bp}) \ , \tag{3}$$

where m_n, r_n, and k_n are the effective mass, damping, and stiffness of bundle n. Thus, each bundle exerts a force on the papilla proportional to the difference in transverse displacement between the bundle and the papilla. Solving Eq. (3) for the velocity V_n of bundle n yields

$$V_n = \frac{1}{1 - \beta_n^2 + i\beta_n/Q_n} V_{\mathrm{bp}} \, , \tag{4}$$

where $\beta_n \equiv \omega/\omega_n$ is normalized frequency, with ω_n and Q_n representing the bundle's resonant frequency and quality factor ($\omega_n \equiv \sqrt{k_n/m_n}$ and $Q_n \equiv k_n/r_n\omega_n$). Substituting Eq. (4) into Eq. (2) and using conservation of mass ($U_{\mathrm{ow}} = A_{\mathrm{bp}}V_{\mathrm{bp}}$) to solve for the input impedance yields

$$Z(\omega) \equiv \frac{P_{\mathrm{v}} - P_{\mathrm{t}}}{U_{\mathrm{ow}}} = \frac{1}{i\omega A_{\mathrm{bp}}^2} \left[Z_{\mathrm{bp}} + \sum_n k_n \frac{-\beta_n^2 + i\beta_n/Q_n}{1 - \beta_n^2 + i\beta_n/Q_n} \right] \, . \tag{5}$$

We introduced micromechanical irregularity into the model by including a small stochastic element in the effective damping of each oscillator (Q_n). Specifically, we took $\tilde{Q}_n = Q_n(1 + \epsilon_n)$, where Q_n is the unperturbed value (see below) and ϵ_n is a small random value close to zero.

3. Analytic Approximation for the Delay

To derive an approximate analytic expression for the emission phase-gradient delay we make several simplifying assumptions (validated using numerical analysis). First, we convert the sum to an integral and neglect spatial variations in bundle stiffness ($k = k_{\mathrm{o}}$). Expressing the integral in terms of β yields

$$\Delta P \approx \frac{U_{\mathrm{ow}}k_{\mathrm{o}}\ell}{\omega A_{\mathrm{bp}}^2} \int_{\beta_0}^{\beta_L} (\epsilon/Q)(Ae^{i\theta})^2 \, d\beta \, , \tag{6}$$

where ℓ is the exponential space constant of the papilla tonotopic map, $\beta_L \equiv \omega/\omega_{\mathrm{min}}$, $\beta_0 \equiv \omega/\omega_{\mathrm{max}}$, and $A(\beta)e^{i\theta(\beta)} \equiv 1/(1 - \beta^2 + i\beta/Q)$ is the transfer function of the harmonic oscillator. Following the analysis of the coherent-reflection model [7], we decompose the irregularity function, $\epsilon(x)$, into spatial-frequency components and assume that the value of the integral is dominated by spatial frequencies in a (relatively) narrow range about some "optimal" value κ_{opt}. The integral then becomes

$$\Delta P \propto e^{-i\kappa_{\mathrm{opt}}\ell \ln \beta_0} \int_{\beta_0}^{\beta_L} \frac{A^2(\beta)}{Q(\beta)} e^{i[\kappa_{\mathrm{opt}}\ell \ln \beta + 2\theta(\beta)]} d\beta \, , \tag{7}$$

(constant terms contributing only to the magnitude have been dropped to simplify the notation). Because the amplitude of the integrand is sharply peaked, the value of the integral does not depend strongly on frequency except near frequencies close to the ends of the tonotopic map. The principal frequency dependence of the emission phase ($\phi \equiv \angle \Delta P$) therefore arises from the argument of the exponential outside the integral and depends on the value of κ_{opt}. We determine κ_{opt} by applying
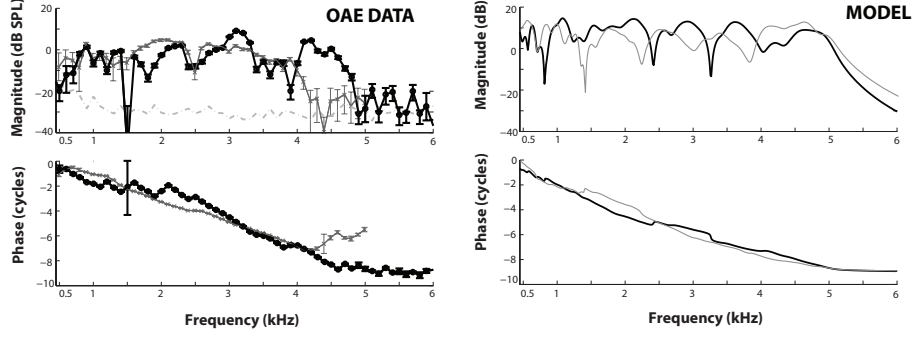
88

Fig. 2: *Left:* Representative SFOAE data at probe levels of 20 dB SPL from both a leopard gecko and tokay gecko [2]. The dashed line shows the acoustic noise floor. *Right:* Model values of $\Delta P(\omega)$ (simulated SFOAEs) based on random micromechanical irregularities. The model papilla comprised 150 bundles with CFs logarithmically distributed from 0.2 to 5 kHz. A roughness factor of 3% was used. Model results are shown for two different "ears" (i.e., different irregularity patterns). The overall model SFOAE magnitude was scaled to approximate that of the measurements.

the principle of stationary phase and requiring that the phase of the integrand be constant near its magnitude peak (i.e., near $\beta \approx 1$). This yields

$$\frac{\partial}{\partial \beta} \left[\kappa_{\mathrm{opt}} \ell \ln \beta + 2\theta(\beta) \right] \bigg|_{\beta=1} = 0 \qquad \Longrightarrow \qquad \kappa_{\mathrm{opt}} = -\frac{2}{\ell} \frac{\partial \theta}{\partial \beta} \bigg|_{\beta=1} . \tag{8}$$

For the harmonic oscillator, one can show that $\frac{\partial \theta}{\partial \beta}|_{\beta=1} = -Q/\pi$. Combining our expressions to compute N_{SFOAE}, the emission phase-gradient delay expressed in stimulus periods ($-\frac{\omega}{2\pi} \frac{\partial \phi}{\partial \omega}$), yields the approximation

$$N_{\mathrm{SFOAE}} \approx \frac{2Q}{\pi} . \tag{9}$$

According to this analysis, the emission phase-gradient delay (in periods) is proportional to the sharpness of tuning.

4. Comparison with Experiment

Figure 2 compares model simulations with published SFOAEs measured in the gecko [2]. The figure shows the magnitude and phase of ΔP computed from Eq. (1) using Eq. (5) for $Z(\omega)$. Parameter values were obtained by assuming that bundle resonant (or characteristic) frequencies (CF) are distributed logarithmically along the papilla [4] with a constant density of oscillators per octave. In the absence of irregularity, the quality factors Q_n were assumed to vary with CF according to the power law $Q_n = 3Q_{10}(\mathrm{CF}_n)$ where $Q_{10}(\mathrm{CF}) = 2.3[\mathrm{CF}/(\mathrm{kHz})]^{0.355}$ is a power-law fit to tuning data obtained from gecko auditory-nerve fibers [4].[a] ϵ_n was randomly sampled from

---

[a]We used the data of Manley et al. [4] but note that gecko ANF Q_{10} values vary considerably across studies. The factor of 3 used to convert to Q_{10} to Q_n is an approximation valid for second-order filters.
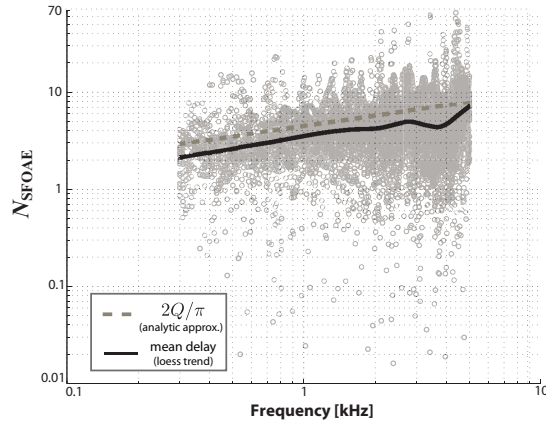
Fig. 3: Model SFOAE phase-gradient delays expressed in stimulus periods. The solid curve is a trend line computed from the results for 20 different simulated ears (grey circles) and trend line (solid line). The analytic approximation given by Eq. (9) is also plotted (dashed line).

a Gaussian distribution with zero-mean and standard deviation 0.03.

As shown in Fig. 2, the model captures many of the qualitative features seen in the emission data. For example, the model reproduces the frequency-dependent variations in SFOAE magnitude, such as spectral notches unique to a particular ear and the high frequency roll-off at frequencies outside the range of the tonotopic map. In addition, both the simulated emissions and the SFOAE data exhibit substantial phase accumulation. These qualitative features are relatively insensitive to model parameters such as the bundle stiffness and the total number of bundles.

When the model Q values are chosen to match ANF responses, the model predicts generally realistic OAE delays. Below 1 kHz, however, the predicted delays are longer than those measured. This low-frequency deviation is similar to that observed in mammals between measures of Q and N_{SFOAE} and may stem from interference between multiple emission source mechanisms. Whereas only one mechanism is represented in the current model, the gecko shows evidence for at least two different OAE generation mechanisms [2]. In both the model and the lizard, substantial SFOAE delays occur despite the absence of BM traveling waves.

Figure 3 demonstrates that the mean phase-gradient delay is well approximated by the analytic expression derived in Eq. (9). Variations in the value of Q along the length of the papilla produce corresponding changes in N_{SFOAE}. These results indicate that the emission phase-gradient delay (N_{SFOAE}) is proportional to the sharpness of tuning (Q).

5. Summary

We have described a simple model for the gecko inner ear in order to predict SFOAE magnitude and phase. When the sharpness of tuning of the model resonators is cho-

90

sen to match ANF responses, the model captures many of the qualitative features of gecko SFOAEs. In particular, the model reproduces the substantial phase-gradient delays in spite of the absence of a tuned BM or traveling waves. The model predicts that SFOAE phase-gradient delays are proportional to the sharpness of tuning of the resonators inside the ear (i.e., the hair cells and associated tectorium). Despite the absence of traveling waves, many mechanisms in the model are qualitatively similar to those of coherent reflection filtering [7] in the mammalian cochlea (e.g., the role of a dominant spatial frequency in determining SFOAE delay). The oscillators used here are presumably too simple (e.g. passive, linear, no fluid coupling between adjacent bundles). Nevertheless, we conjecture that the proportionality between SFOAE delays and sharpness of tuning described here holds in more realistic models.

Acknowledgments

References

1. Shera, C.A., Guinan, J.J. Jr., Oxenham, A.J., 2002. Revised estimates of human cochlear tuning from otoacoustic and behavioral measurements. Proc. Natl. Acad. Sci. 99, 3318–3323.
2. Bergevin, C., Freeman, D.M., Saunders, J.C., Shera, C.A., 2008. Otoacoustic emissions in humans, birds, lizards, and frogs: Evidence for multiple generation mechanisms. J. Comp. Physiol. A 194, 665–683.
3. Peake, P.T., Ling, A. Jr., 1980. Basilar-membrane motion in the alligator lizard: its relation to tonotopic organization and frequency selectivity. J. Acoust. Soc. Am. 67, 1736–1745.
4. Manley, G.A., Koppl, C., Sneary, M., 1999. Reversed tonotopic map of the basilar papilla in Gekko gecko. Hear. Res. 131, 107–116.
5. Aranyosi, A.J., Freeman, D.M., 2004. Sound-induced motions of individual cochlear hair bundles. Biophys. J. 87, 3536–3546.
6. Rosowski, J.J., Peake, W.T., Lynch, T.J., Leong, R., Weiss, T.F., 1985. A model for signal transmission in an ear having hair cells with free-standing sterocilia. II. Macromechanical stage. Hear. Res. 20, 139–155.
7. Zweig, G., Shera, C.A., 1995. The origin of periodicity in the spectrum of evoked otoacoustic emissions. J. Acoust. Soc. Am. 98, 2018–2047.
8. Miller, M.R., 1973. A scanning electron microscope study of the Papilla basilaris of *Gekko gecko*. Z. Zellforsch. 136, 307–328.
9. Wever, E.G., 1978. The Reptile Ear. Princeton University Press.
10. Shera, C.A., Guinan, J.J. Jr., 2003. Stimulus-frequency-emission group delay: A test of coherent reflection filtering and a window on cochlear tuning. J. Acoust. Soc. Am. 113(5), 2762–2772.